Optical coherence tomography for glucose monitoring in blood

Hafeez Ullah[1,2] · Fayyaz Hussain[3] · Masroor Ikram[2]

Abstract In this review, we have discussed the potential application of the emerging imaging modality, i.e., optical coherence tomography (OCT) for glucose monitoring in biological tissues. OCT provides monitoring of glucose diffusion in different fibrous tissues like in sclera by determining the permeability rate with acceptable accuracy both in type 1 and in type 2 diabetes. The maximum precision of glucose measurement in Intralipid suspensions, for example, with the OCT technique yields the accuracy up to 4.4 mM for 10 % Intralipid and 2.2 mM for 3 % Intralipid.

1 Introduction

OCT is a high-resolution imaging modality that uses low-coherence interferometry (LCI) techniques (in situ and real time) [1] with the axial resolution of 1–15 μm to perform high-resolution imaging of biological tissues, especially imaging of transparent tissues [2, 3] up to depth of 2 mm. The tissue surface can be scanned by moving the light beam latterly on sample to achieve two-dimensional images with ultrahigh resolution [4]. In Doppler (D-OCT), the precision of the Doppler frequency due to speckle modulation for the flow velocity of the backscatterers spectrum in Brownian motion is often effected [5]. This leads toward glucose monitoring in turbid media with the temporal analysis of OCT under dynamic light scattering (DLS) [6, 7].

For prerequisite control of glucose in diabetes, blood drop is obtained by pricking the finger making it unpleasant and painful. Therefore, it is necessary to introduce a non-invasive method for monitoring of glucose from skin that could offer a wonderful relief to diabetic's patients [8, 9]. These methods include optical methods, ultrasonic, impedance, and heat capacitance [10, 11]. But in these methods, the measurements may differ based on skin morphology and biophysical characterizations due to the complex structure of skin with a nonuniform vascularization, thus relying only on the upper skin layers (epidermis and upper dermis) [8].

Therefore, the development of the techniques for monitoring and quantification of the molecular diffusion in blood vessels has resulted in advancements of the novel therapeutic agents, drug delivery techniques, and novel clinical diagnostic methods [12]. Many techniques for this purpose have been in practice such as spectrophotometry, spectrofluorometry, fluorescence microscopy, microdialysis, polarimetry [13], Mach–Zehnder interferometric waveguide [14], Raman spectroscopy, near-infrared absorption, and scattering and photoacoustics [15, 16]. These techniques include some limitations such as low sensitivity, specificity, and accuracy at physiological glucose measurements [17]. OCT has been deemed to be applied in functional imaging, monitoring, and quantification of diffusion processes making it important for in vitro and in vivo applications. OCT has monitored and quantified the depth-resolved diffusion of glucose more efficiently than previously reported techniques [12].

It has been reported previously that the addition in the glucose concentration causes the changes in protein

✉ Hafeez Ullah
hafeezullah79@gmail.com

1   Laser and Optronics Laboratory, Department of Physics, Bahauddin Zakariya University, Multan 60800, Pakistan

2   Department of Physics and Applied Mathematics, Pakistan Institute of Engineering and Applied Sciences, Nilore, Islamabad, Pakistan

3   Material Simulation Research Laboratory (MSRL), Department of Physics, Bahauddin Zakariya University, University Campus, Bosan Road, Multan 60800, Pakistan

Fig. 1 OCT data from healthy pig aorta **a** structured OCT image, and **b** corresponding OCT signal (reprinted with permissions [29])
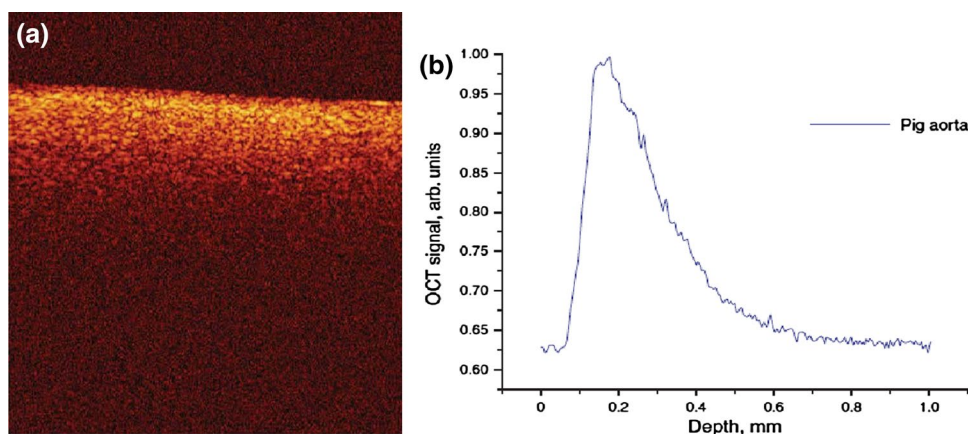
(collagen, myosin) [18], i.e., 18 mg/dl glucose affects ~20 % in the OCT signal [16, 19]. The first experiment of OCT in noninvasive glucose monitoring was conducted by University of Texas's group [20] with the accuracy of ~1 mM very close to applicable in human physiological levels. In the strongly scattering media, $\mu_s \gg \mu_a$; hence, the information can be extracted by analyzing the OCT signal for scattering coefficient only. Some groups have analyzed these OCT methods with simulations of phantom studies such as Kirillin et al. [21] show a 7 %/1000 mg/dl change in simulations for 5 % Intralipid. Kinnunen et al. [22] show a 2.1 %/30 mM change in 2 % Intralipid and a 0.86 %/30 mM change in 5 % Intralipid. Their in vitro study shows changes between 20 and 52 %/30 mM in different mouse skin samples. Larin et al. show a 0.023 %/1 mM change in polystyrene microsphere suspension and a 0.032 %/1 mM change in 3 % fat milk [23, 24]. Their in vivo study also shows a 3.3 %/mM change in the rabbit ear, a 2.3 %/1 mM change in the micropig skin [24, 25], and a change of 3.4 %/1 mM in human subjects [26]. This reflects the success of OCT as a noninvasive technique to monitor maximum precession of glucose measurement in 3 and 10 % Intralipid suspensions [24] with greater sensitivity [27]. Thus, OCT has been proved to be the reliable methodology in diabetes to increase the efficacy and a guide in medical nutrition therapy and exercise.

1.1 OCT: a glucose sensor

The OCT signal obeys the exponential law for its total attenuation coefficient due to scattering and absorptions because $\mu_t = \mu_a + \mu_s$. If $\mu_a \ll \mu_s$, then only scattering (ballistic) photons are enough to explore the change in optical properties due to refractive index change of scattering centers (like cell membranes, cellular components, and protein aggregates), n_s, and interstitial fluid (ISF), n_{ISF}, for the analysis of exponential profile of OCT signal. The ratio of refractive indices is then $\Delta n = n_s / n_s n_{ISF}. n_{ISF}$. The

10 mg/dl increase in glucose increases n_{ISF} by a factor of 1.52×10^{-5}, and consequently, n_s is decreased by decreasing the index mismatch $\Delta n = \frac{n_s}{(n_{ISF} + 1.52 \times 10^{-5}/10 mg/dl)}$ [26].

Skin consists of three major layers: a dead keratinized layer of squames (stratum corneum of the epidermis), a prickle cells layer (epidermis), and a connective tissue of dermis (where blood microvasculatures are present in network) [28]. The highly resolved OCT signal is mainly detected from dermis area of the skin after changing the glucose concentration in *ISF* as noninvasive monitoring [19]. For glucose monitoring with OCT, the structured OCT images (Fig. 1a, for example) are averaged into a single 1D distribution of light in depth on logarithmic scale (Fig. 1b) where we are able to get information about the change in the optical parameters such as scattering by analyzing the profile of light attenuation [29].

1.2 M-mode scanning of swept source-OCT for glucose quantification

DLS or ballistic photon (single) scattering underlying Brownian motion can be analyzed using swept source (SS-OCT) in M-mode scanning [30] to quantify the glucose levels in fluids. Two types of motions are associated with a particle under Brownian motion in turbid media: (i) translational relaxation and (ii) rotational relaxation. The translational relaxation or decorrelation time provides the source of contrast between liquid and solid tissues. These quantitative data are baseline for glucose monitoring and translating it toward in vitro and in vivo environment where blood viscosity can be measured to quantify glucose levels. SS-OCT glucose sensor is based on the Brownian motion.

Consider a spherical particle executing Brownian (random) motion in a liquid. The time of motion and path are divided into small intervals so that the resultant displacement is the mean-squared displacement, and the particle distribution is Gaussian. We denote the displacement $\langle \Delta r^2(t) \rangle = 6D_T \tau_T$ for diffusing particles [31]. Here, D_T is

called translation diffusion coefficient, τ_T is translational relaxation or decorrelation time and is related by the following equation,

$$\tau_T = \frac{1}{2k^2 D_B}. \tag{1}$$

This Brownian motion underlies the phenomena of DLS by measuring intensity fluctuations arising from phase and/or amplitude of a single-scattered electromagnetic field due to particle dynamics.

1.3 M-mode scanning of SS-OCT in stagnant blood

SS-OCT based on Brownian motion has been applied for measuring glucose in liquid phantoms and whole blood (in vitro) by measur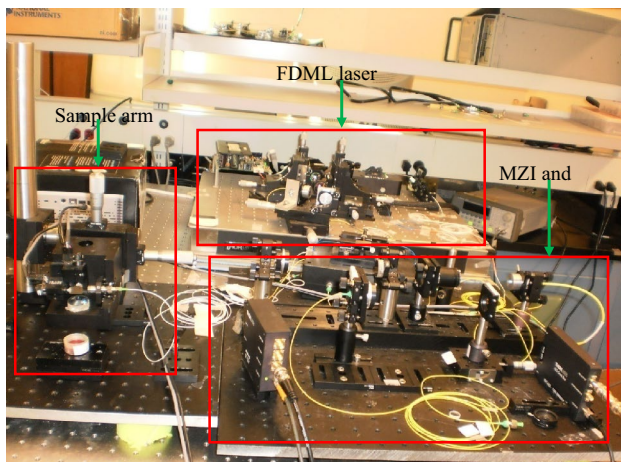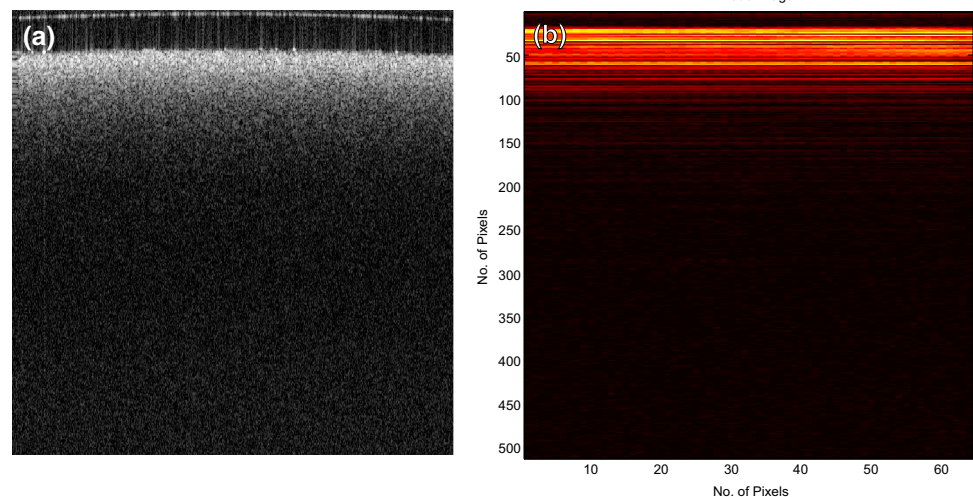ing the temporal dynamics of light scattering. The addition of glucose affects the Brownian motion of red blood cells (RBCs) in blood [7]. Whole blood with asymmetric RBC scatterers drawn from 5-month-old Lewis rats was admixed with additional glucose to 0, 20, 40, 60, and 80 mM levels [7]. A custom built 36 kHz SS-OCT system has been used for M-mode measurements [7] (measurements of OCT data with respect to time) scanning similar to that described by Mariampillai et al. [32]. Figure 2 shows the snapshot of the experimental setup during M-mode measurements of a typical blood sample. Briefly, the SS-OCT system consists of frequency domain mode locking (FDML) fiber-ring laser source comprising of polygon-based tunable filter. The FDML configuration consists of total cavity length of 3.3 to 4.5 km. A fiber Bragg grating is used for A-scan (depth scan) triggering. The coherence length and spectral sweeping range were 6 mm and 112 nm, respectively, at a central wavelength of 1310 nm. The axial resolution in tissue and the average output power of the system were 8 μm and 48 mW [7, 33].

For M-mode analysis, the signal was investigated at the depth below 70 μm because this depth is free from any possible surface distortions or artifacts, and offers the measurement of ballistic scattering [34]. OCT images for a typical glucose concentration of 80 mM in whole blood are shown in Fig. 3. Figure 3a depicts a raw 2D OCT image (640 × 512 pixels and 5 mm × 2 mm, width × depth), and Fig. 3b shows an M-mode 2D OCT image with (64 × 512 pixels and 0 mm × 3 mm, width × depth) [33]. Consecutive 64 A-scans were combined to obtain average signal intensity (M-mode point, resulting in ~3.6 ms spacing) for 5 s at the same central sample lateral location. The experiment temperature was 21 °C [7].

Fig. 2 Photograph for M-mode scanning with SS-OCT of a typical blood sample [33]

Fig. 3 Swept source-OCT images: **a** structural 2D OCT image with pixels (640 × 512) and dimensions (5 mm × 2 mm) along x- and z-axis for blood with 80 mM glucose in it and **b** an M-mode 2D OCT image with (64 × 512) pixels and dimensions (0 mm × 3 mm) along x- and z-axis (self research work [33])
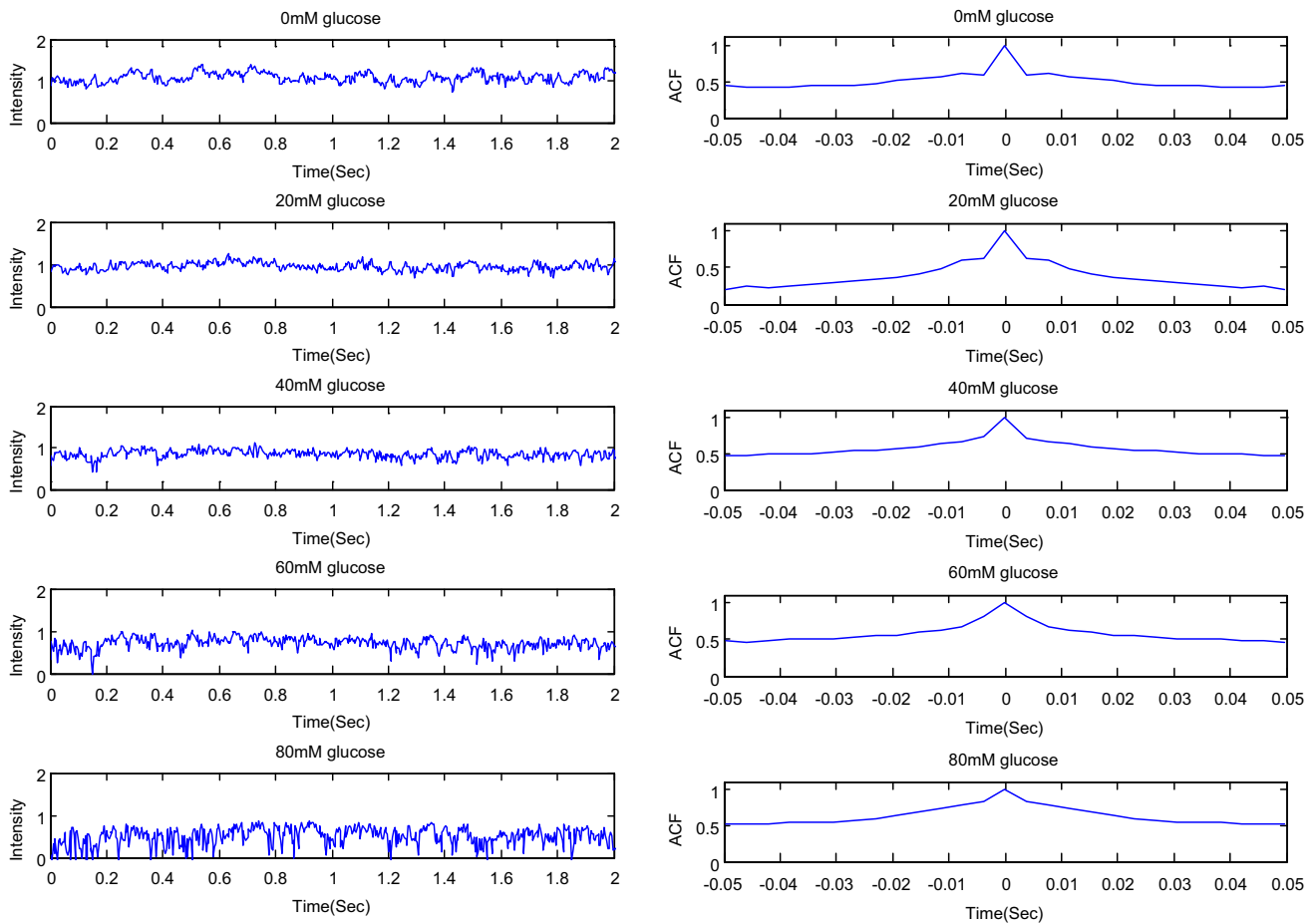
Fig. 4 a OCT M-mode intensity signals at a depth of 70 µm for six different glucose concentrations in the whole-blood phantom at 21 °C, **b** signal autocorrelation functions (ACF) obtained from the OCT M-mode data of "a" with Eq. (3) (self research work [33, 41])

1.3.1 M-mode signal processing

The signal recorded at the detector of the SS-OCT system is given by [7, 35],

$$I_D = \frac{1}{2} \int_0^\infty I_{so}(k)(1 + \cos kx)\mathrm{d}k = \frac{1}{2}I_{so} + \frac{1}{4}\int_{-\infty}^\infty I_{so}(k)e^{ikx}\mathrm{d}k, \tag{2}$$

where x is the path length difference, $I_{SO}(k)$ is the source intensity, and the integral $\int_0^\infty I_{so}(k)e^{ikx}\mathrm{d}k$ is called autocorrelation function (ACF). The power spectrum $P(\omega)$ and ACF are related by Weiner–Khinchin theorem as a Fourier pair:

$$\mathrm{ACF}(x) = \int P(\omega)e^{-i\omega x/c}\mathrm{d}\omega. \tag{3}$$

The raw M-mode OCT intensity signals as a function of time at a depth of 70 µm for six different glucose concentrations c_{gl} were obtained for whole blood consisting on the data train of 1400 OCT intensity points 3.6 ms apart

depicting the effect of decrease in refractive index mismatching between medium and scatterers. For illustrative purpose, Fig. 4a depicts this intensity up to ~2.0 s. The ACF was extracted according to Eq. (3) for the six different glucose concentrations is shown in Fig. 4b. It is seen that increasing glucose levels causes longer OCT signal relaxation decays, as expected from the slower Brownian motion of scattering particles in the media of increasing viscosity [7].

In the presence of asymmetric RBCs in blood, a double exponential fit $[f_2 = B * \exp\left(-t/\tau_T^/\right) + C * \exp\left(-t/\tau_R\right)]$ to account for both translational and rotational relaxations was applied to the OCT's ACFs. Where $\tau_T^/$ and τ_R are the translational and rotational decorrelation times of erythrocytes. If we approximate RBCs as a flattened ellipsoid of radius R and half the average thickness a, in analogy with Eq. (1) [7, 31], then

$$\tau_T^/ = \frac{1}{2k^2 D_T^/} \quad \text{and} \quad D_T^/ = \frac{k_B T}{6\pi \eta a}G(\rho) \tag{4}$$

where G is a geometrical factor given by $G(\rho) = \left(\rho^2 - 1\right)^{1/2} \times \rho \times \arctan\left(\rho^2 - 1\right)$ and $\rho = \frac{R}{a} > 1$.

Table 1 Summary of the OCT experimental results and analysis for the stagnant whole-blood sample, demonstrating the quantification of glucose-induced viscosity changes (self research work [7])

Sample glucose concentration (mM)	Translational decorrelation time (ms)	Viscosity: from Eq (4) for sample set whole blood (mPa.s)	r^2 value
0	8.20 ± 0.04	9.03	0.93
20	9.52 ± 0.08 (8.41 ± 0.04)	10.26	0.99
40	12.00 ± 0.05 (10.40 ± 0.06)	10.81	0.91
60	26.30 ± 0.13 (12.2 ± 0.06)	24.61	0.93
80	63.00 ± 0.40 (25.00 ± 0.14)	51.05	0.99

Table 2 OCT experimental results for the flown whole-blood phantom, demonstrating the quantification of glucose-induced diffusion coefficient changes (self research work [6])

Sample glucose concentration (mM)	Translational decorrelation time (ms)	Translational diffusion coefficient (m^2/s)	r^2 value
0	34.01 ± 0.69	8.65×10^{-14}	0.99
20	46.30 ± 0.40	6.39×10^{-14}	0.99
40	58.12 ± 0.55	5.06×10^{-14}	0.99
60	68.43 ± 0.57	4.31×10^{-14}	0.99
80	129.02 ± 0.94	2.27×10^{-14}	0.99

Table 3 Comparison of flown whole-blood results with the results of stagnant whole blood (self research work [6, 7])

Sample glucose concentration (mM)	Translational diffusion coefficient static fluids (m^2/s)	Translational diffusion coefficient flowing fluids (m^2/s)	Flowing/static ratio
0	3.59×10^{-13}	8.65×10^{-14}	0.24
20	3.09×10^{-13}	6.39×10^{-14}	0.21
40	2.45×10^{-13}	5.06×10^{-14}	0.21
60	1.12×10^{-13}	4.31×10^{-14}	0.39
80	4.65×10^{-14}	2.27×10^{-14}	0.49

For a red blood cell, $R = 3.5$ μm and $a = 1.0$ μm [7], $k = 4\pi n/\lambda$ is the wave number, n is the refractive index, k_B is Boltzmann constant, T is absolute temperature, and η is the viscosity of the medium.

Table 1 summarizes the derived translational decorrelation times τ_T' for blood sample, the resulting viscosities η, and the fitting correlation coefficients r^2. The brackets include the decorrelation time results of a control experiment in the data set of blood sample set due to long exposure of blood to the air during the measurements. Despite the many complexities associated with whole-blood analysis, the increasing trend of medium viscosity with added glucose levels is observed. The derived viscosity value for the blood sample without added glucose, i.e., $\eta_{blood} = 9.03$ mPa. s also agrees well with the literature value of 10 mPa. s [36, 37].

1.3.2 M-mode scanning of SS-OCT in flown blood

The effect of blood flow (forced convection) has been explored with the same apparatus and the same signal processing [7] in capillaries where slow velocity rates of ~mm/s, shorter decorrelation rates are expected and reliably measured on the basis of diffusion coefficients. By quantifying the glucose levels in flowing blood, eventually, it is envisioned a blood vessel by speckle variance (SV-OCT) to further examine in M-mode, with ACF analysis. Ullah et al. [6] have investigated whole blood flowing under the action of gravity through a 600-μm-inner-diameter polymer capillary tube.

Table 2 contains the quantitative parameters including derived translational decorrelation times for diffusion coefficients and the fitting correlation coefficients r^2 for flown whole blood. Table 3 compares the flowing-fluid findings with previous results for nonflowing phantoms [6].

It is reassuring to note that the value of D'_T for whole blood (without added glucose) agrees well with the literature, where a translational diffusion coefficient of ~6.5×10^{-14} m^2/s is reported [6, 38]. Comparing Table 3, one would expect the presence of flow results in an apparent slowing of the decorrelation process, yielding slower
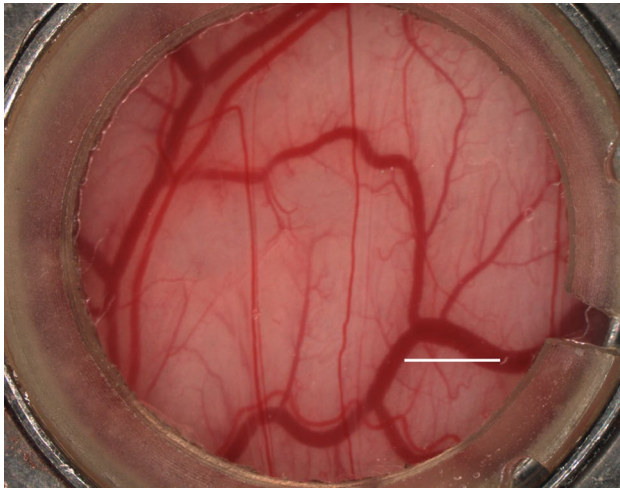
Fig. 5 White light microscopy image of window chamber model that delineates the blood vessels of a female nude mouse for SV-OCT mapping. *Scale bar* 2 mm [33, 41]

Fig. 6 A conceptual diagram of an acquired speckle variance data set of N frames and corresponding indices used to label the frame (i), transverse pixel location (j), and the axial pixel location (k) [33, 40]

diffusion coefficients compared to the static case (D_T ratios less than unity, in the 0.2–0.5 range) [6, 39].

1.4 M-mode scanning for in vivo blood glucose quantification

SV-OCT has been utilized to map out the blood microvasculature in three dimensions for the monitoring of the glucose levels in blood after analyzing the Brownian motion of erythrocytes underlying DLS. The technique has been applied on nude live mouse's skin for which the microscopic images have also been obtained for normal blood vessels using dorsal skinfold mouse windows chamber (DS-MWCM) [33, 40, 41]. The crucial parameter required for SV-OCT includes the minimization of tissue motion artifacts; therefore, DS-MWCM provides a stationary platform (free from bulk motion) and has been implanted on a nude mouse. In Fig. 5, the white light microscopy image of window chamber model has been depicted for illustration purpose that delineates the blood vessels for SV-OCT mapping [33, 40, 41].

1.4.1 Animal model

Before applying the DS-MWCM, the mouse was anesthetized with a ketamine–xylazine (90–10 mg/kg) mixture. A 10-mm-diameter region of skin is placed between the titanium plates of DS-MWCM. A 12-mm-diameter and 250-μm-thick coverslip is used to protect the exposed fascia and vasculature. OCT imaging was performed by fixing the DS-MWCM into the removable light weight aluminum plate to keep the animal at 37 °C after the recovery of the animal from surgery [33, 40, 41]. In this study, five
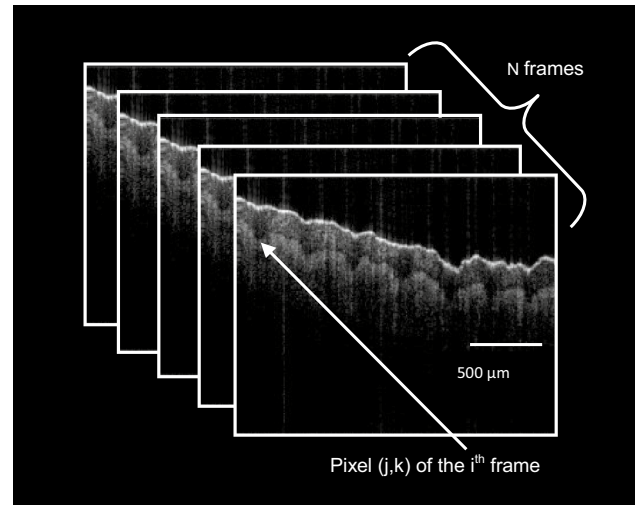
animals were investigated and the diffusion coefficient was averaged.

1.4.2 SV-OCT and M-mode imaging system

OCT data were obtained from 36 kHz SS-OCT system as described earlier for in vitro case scenario [33, 40]. The interframe OCT fluid contrast algorithm termed as SV-OCT is based on the idea that the image speckle/texture of relatively solid regions will persist between consecutive images, whereas speckle will show greater interimage speckle washout in regions of greater fluidity [42]. The algorithm for the generation of speckle variance images of OCT data needs to calculate the variance of pixels from a set of N, B-mode images (N is gate length), acquired from the same spatial location [33, 40, 41],

$$SV_{ijk} = \frac{1}{N} \sum_{i=1}^{N} \left(I_{ijk} - \frac{1}{N} \sum_{i=1}^{N} I_{ijk} \right)^2. \tag{5}$$

where i, j, and k are indices for the frame (up to N), transverse, and axial pixels, and I is the corresponding pixel intensity value at the imaging speeds of 20 frames per second. A more clearly schematic representation of the data set and pixel indices for three-dimensional frames stacking according to Eq. (5) is shown in Fig. 6. Figure 7 shows a blood vessels image of normal nude mouse obtained with SV-OCT. This 3D processed image of blood microvasculature shows the distinction between the individual blood vessels with the dimensions of 6 mm × 6 mm × 2.2 mm [33, 40, 41].

Fig. 7 SV-OCT microvasculature image of a normal mouse in DS-MWCM, a low bulk tissue motion situation with gate length $N = 8$. Dimensions: (6400 × 1520 × 512, pixels) and/or (6 mm × 6 mm × 2.2 mm). The ROI is represented with magnification, and depth-encoded color bar used to specify the depth of the vessel. *Scale bar*: 250 μm [33, 40]
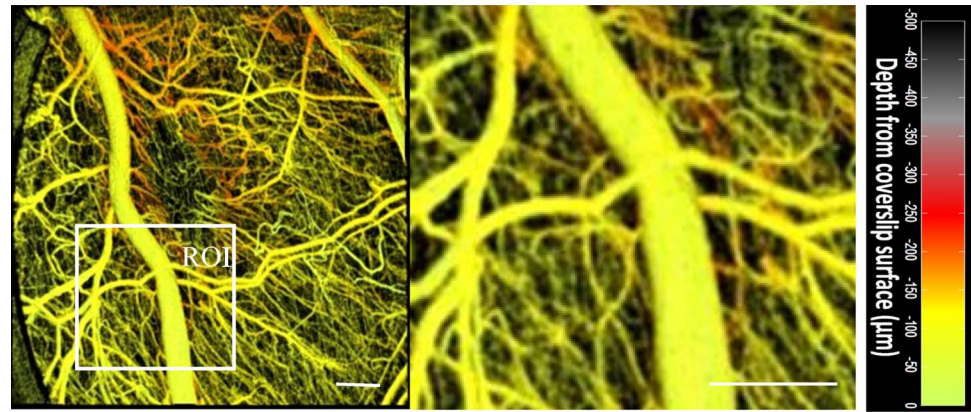

Table 4 Summary of Brownian motion analysis results in dynamic light scattering regime including translational decorrelation time, translational diffusion coefficient, and r^2 values for all five animals [33, 40, 41]

Animals	Translational decorrelation time (ms)	Translational diffusion coefficient (m²/s)	r^2 value
Animal 1	38.20	1.02×10^{-14}	0.93
Animal 2	44.00	6.68×10^{-14}	0.95
Animal 3	48.80	6.03×10^{-14}	0.98
Animal 4	46.70	6.30×10^{-14}	0.99
Animal 5	52.20	9.20×10^{-14}	0.96
Average	45.98	5.85×10^{-14}	0.96

Therefore, the SV-OCT image was used to select the ROI for in vivo study of glucose monitoring in five animals. With the help of M-mode imaging, the average value of D_T was yielded ~5.85×10^{-14} m²/s (Table 4). The only 10 % difference was observed from theoretical value of diffusion coefficient (5.85×10^{-14} vs. 6.50×10^{-14} m²/s [38]). The reason for this difference may include the forced convection, shear effect, and technique employed for measurements. A clearer 3D image of glucose-free mouse's microvasculature bed helps to visualize the suitable blood microvessels and provides easy selection of the ROI to obtain M-mode data (Fig. 7). In this way, the threshold measurement to quantify glucose levels for in vivo case scenario of injected higher glucose concentrations intravenously has been achieved [33, 40, 41].

1.5 Affinity-based turbidity glucose monitoring sensor

For the construction of highly specific turbidity glucose monitoring sensor, a layer is created using a sensor chemistry composed of small spherical hydrogel particles. Concanavalin A (ConA) is used to act as scattering medium as a function of glucose concentration in the presence of refractive index mismatch effect. The OCT setup in this technique consists of SLD light source ($\lambda_0 = 1.3$ μm, P = 500 μW, and l_c ~14 μm). In this setup, the continuous wave light-emitting diode (CW LED, $\lambda = 1.3$ μm) is used as aiming beam. The output power incident on the sample is 200 μW. A photodiode is used to detect the interferogram signal. This signal is then preamplified, electronically filtered on resonance Doppler-shifted frequency ($f_D = 700$ kHz), amplified by a logarithmic amplifier (dynamic range 0–100 dB, amplification coefficient 23 mV dB-1, noise level 5–10 dB without averaging, and ~0.2 dB with averaging of 512 spatially independent signals every 9 s [34]), visualized with a digital oscilloscope, digitized by an analog-to-digital converter (ADC), and recorded by a data logger for further processing. The sensorgram, i.e., OCT signal scanned the area ~0.2 mm × 0.2 mm in 1-mm path length cuvette. A typical OCT sensorgram of the sensor inside the cuvette is shown in Fig. 8 [43].

1.6 OCT signal slope (OCTSS) and OCT amplitude (OCTA) methods

1.6.1 Glucose monitoring in rabbit and monkey eyes

The TD-OCT has been utilized for depth-resolved monitoring of glucose diffusion in fresh rabbit eyes (16 for whole experiment) in which the OCT system consists of a low-coherence broadband light source ($\lambda = 1310 \pm 15$ nm, $P_{out} = 375$ μW, and resolution of 25 μm) by Ghosn et al. [12]. The tissue is illuminated with laterally scanning (2.2 mm × 2.4 mm) endoscopic probe. Total consumed time

Fig. 8 Principle of measuring reversible glucose-dependent turbidity change in the ConA/ Sephadex dialysis sensor (thickness approximately 0.4– 0.6 mm) in a cuvette by OCT filled with 0 and 30 mM glucose solutions added (reprinted with permission from American Chemical Society, 2013 [43])
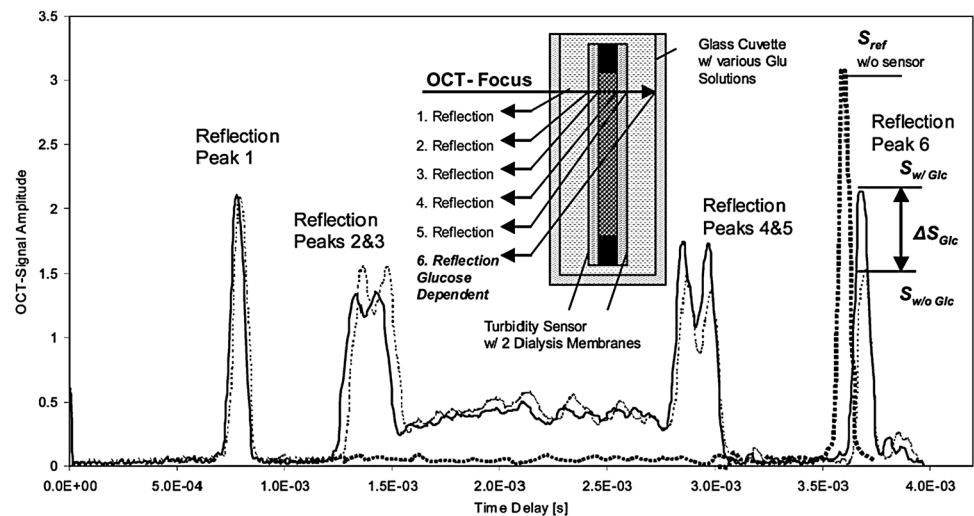
is 90–150 min with the average rate of 3 s per image. 1D attenuation OCT signal is obtained by averaging the lateral direction to get depth profile on logarithmic scale. The sample is stored in a 0.9 % NaCl solution (pH 5.5) at 22 °C. A 20 % glucose solution in saline is prepared by adding 4 ml of a 40 % glucose solution to the sample in saline after 10 min from the starting point. Two methods have been used to calculate the permeability coefficient: (i) OCT signal slope (OCTSS) and (ii) OCT amplitude (OCTA) methods. The average permeability coefficient $\acute{P}_G$ is calculated with OCTSS method by dividing the thickness of the region used to calculate the OCTSS (~155–255 μm) by the time of glucose diffusion inside this region, i.e., $\acute{P}_G = z_{region}/t_{region} = 9.49 \times 10^{-6}$ cm/s (Fig. 9). The time is calculated as the time when the saturation stage is reached minus the time when the OCTSS started to change (highlighted by a box). On the other hand, OCTA method calculates $\acute{P}_G(z) = z_i/t_{zi}$ at specific depth z_i, where t_{zi} is the time of glucose diffusion to this depth (starting from adding of glucose up to the changes in OCT amplitude commenced). z_i is calculated from the epithelial surface of the sclera to the specific depth in sclera stroma. The thickness and refractive index of the sclera are 349 μm and 1.4, respectively, but for measurements, the used thickness was 210, ~36 μm below the epithelial surface. The typical OCT signals calculated from different depths of tissue are shown in Fig. 10a. The typical permeability coefficients measured at different depth can be seen in Fig. 10b by OCTA method which is seen to be nonlinear increasing from $2.39 \pm 0.73 \times 10^{-6}$ cm/s at the epithelial side to $8.63 \pm 0.27 \times 10^{-6}$ cm/s close to the endothelial side of the sclera [12].

The same TD-OCT system has been used to monitor glucose in epithelial tissues (rabbit and monkey eyes; porcine skin; and coronary artery) by Larin et al. [44]. For isolated rabbit sclera during water diffusion experiments, the results are expressed in Fig. 11 where OCT signal slope has been
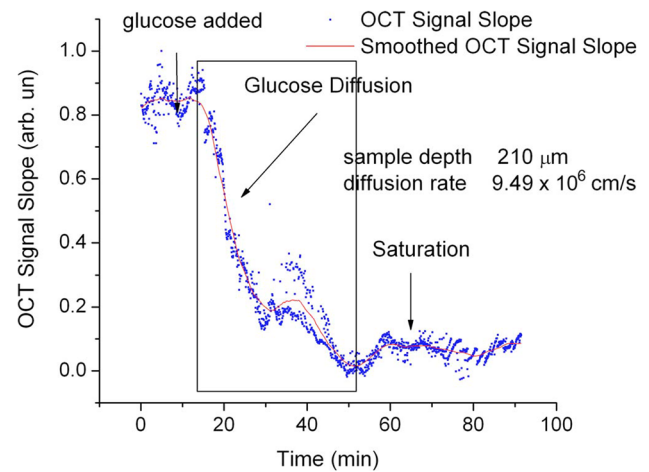

Fig. 9 Temporal analysis of OCT signal slope during the glucose diffusion experiment of sclera (reprinted with permission [12])

calculated from the 279-mm region at a sclera depth of approximately 105 mm from the surface. From Fig. 7, the water permeability rate, P_{isol}^W ~6.6 × 10⁻⁵ cm/s, has been explored for cornea during glucose diffusion experiment. The OCT signal slope shown in Fig. 12a was calculated from the 175-mm region at the corneal (partly submerged) depth of approximately 350 mm from the epithelial surface which yielded permeability coefficient = 1.62×10^{-5} cm/s. For fully submerged eyeballs, the OCT signal slope is shown in Fig. 12b resulting in glucose permeability coefficient ~5.5×10^{-6} cm/s. In vitro results for permeability coefficient from glucose diffusion studies in a typical pig skin are shown in Fig. 12c from which the calculated permeability coefficient is ~8.95×10^{-6} cm/s but the average glucose permeability in pig skin in vitro is ~$(7.69 \pm 0.56) \times 10^{-6}$ cm/s [44].

Ghosn et al. [45] also have used the aforementioned OCT system for glucose monitoring in rhesus monkeys

Fig. 10 **a** OCT signal from different depths of the tissue. The starting of glucose diffusion is denoted by *arrows* at the particular depth and **b** diffusion rates measured at different depths in the sclera (reprinted with permissions [12])
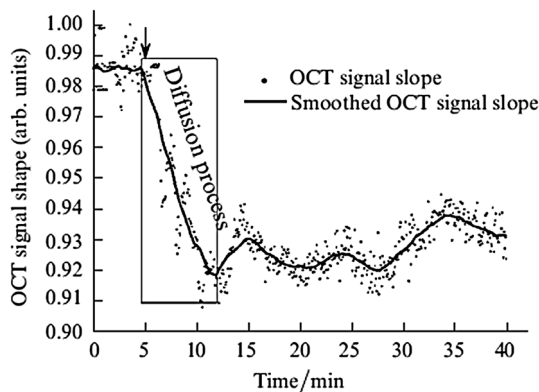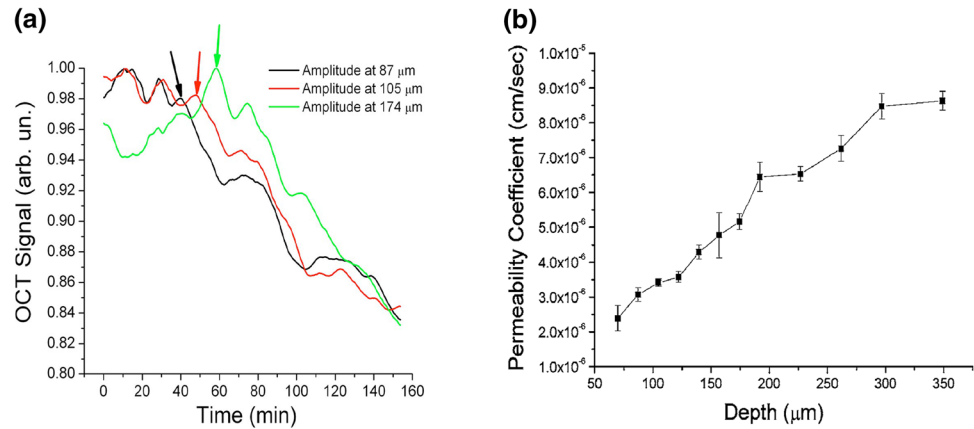

Fig. 11 OCTSS as a function of time recorded from isolated sclera during water diffusion experiment (reprinted with permissions [44])

(Macaca mulatta) where small changes occurred have been detected due to scattering induced by the molecular movement flux. 0.2 ml of 20 %-concentrated glucose (diluted in distilled water; refractive index–1.35, pH–4.6) is topically applied through the hole in the probe holder during the course of imaging, and its diffusion in the skin is monitored with OCT. OCTSS method is used for the calculation of the permeability rate of glucose in monkey skin [12, 25, 46]. After addition of the glucose, the effect of water washout from the dermis due to the hyperosmotic properties of glucose is significant causing the refractive index matching of the scatterers and the ground (interstitial) material. This causes the decreases in the OCT signal slope as a function of time. From these experiments, the averaged permeability rate of glucose from four different monkeys has been evaluated to be $(4.41 \pm 0.28) \, 10^{-6}$ cm/s [45].

While using the same TD-OCT system for fresh New Zealand white rabbit eyes (stored in 0.9 % sodium chloride solution to prevent dehydration), the OCT images were continuously acquired for 60–180 min to calculate the permeability coefficient by Ghosan et al. [46]. Ophthalmic drugs studied in this experiment were metronidazole,

ciprofloxacin, dexamethasone, and mannitol with respective concentrations of 0.5, 0.3, 0.2, and 20 %, respectively. Two methods, OCTSS and OCTA, have been used to calculate the permeability coefficient. The permeability coefficient for water is found to be $(1.68 \pm 0.54) \times 10^{-5}$ cm/s. Ciprofloxacin (0.3 %), dexamethasone (0.2 %), and metronidazole (0.5 %) had permeability coefficients of $(1.85 \pm 0.27) \times 10^{-5}$, $(2.42 \pm 1.03) \times 10^{-5}$, and $(1.59 \pm 0.43) \times 10^{-5}$ cm/s, respectively. Table 5 shows the summary of the permeability coefficients of different agents in the rabbit cornea. The permeability coefficient of water was found to be $(1.33 \pm 0.28) \times 10^{-5}$ cm/s. Ciprofloxacin, mannitol, glucose 20 %, and metronidazole had permeability coefficients of $(1.41 \pm 0.38) \times 10^{-5}$, $(6.18 \pm 1.08) \times 10^{-6}$, $(8.64 \pm 1.12) \times 10^{-6}$, and $(1.31 \pm 0.31) \times 10^{-5}$ cm/s, respectively. Table 6 gives the permeability coefficients of these agents in sclera [46].

Larin et al. [47] have also used OCT to monitor the glucose in fresh coronary arteries from pigs performed within 24 h after obtaining from the source at 22 °C. In this experiment, 20 % glucose solution was examined for 1 h. The OCT signal slope was calculated from 105-μm region at tissue depth of approximately 52 μm from the surface. The calculated averaged permeability rate was $1.43 \pm 0.24 \times 10^{-5}$ (cm/s).

Gosan et al. [48] reported the permeability coefficient of dextran tetramethyl rhodamine in pig aortas chilled 0.9 % saline solution using OCT. From the OCTSS graph for a pig aorta during this dye diffusion experiment, the permeability rate was computed to be 2.59×10^{-5} cm/ s. The permeability rate of the dye was found to be $(2.45 \pm 0.46) \times 10^{-5}$ cm/s (for $n = 3$ experiments) [48].

The OCT system consisting of an SLD ($\lambda_0 = 1310$ nm, $\Delta\lambda = 50$ nm, axial resolution 10–15 μm, transverse resolution of about 25 μm) applied on esophageal tissues of size 1.5×1.5 cm^2 with thickness varying from 1.0 to 3.0 mm after performing esophageal cancer surgery by Zhao et al. [49]. The permeability coefficient of 40 %
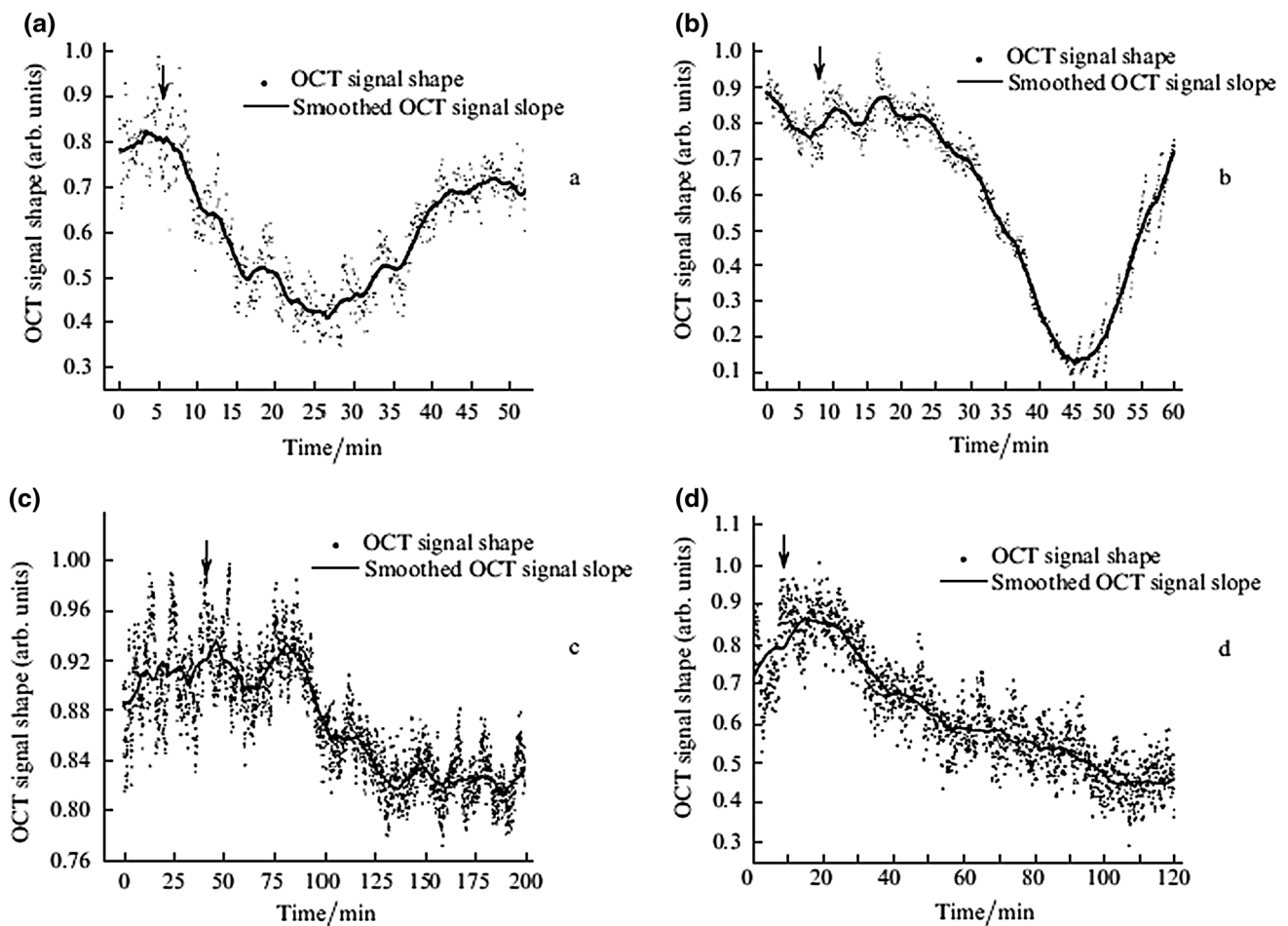
Fig. 12 OCTSS as a function of time recorded from cornea in partially submersed whole eyeballs **a**, in fully submersed whole eyeballs **b**, from pig skin (in vitro) **c,** and from monkey skin (in vivo) **d** during glucose diffusion experiment (reprinted with permissions [44])

Table 5 Permeability coefficient of different agents in rabbit cornea [46]

Agent	Permeability coefficient ± SD (cm/s)	No. of independent experiments
Water	$(1.68 \pm 0.54) \times 10^{-5}$	8
Ciprofloxacin	$(1.85 \pm 0.27) \times 10^{-5}$	4
Mannitol	$(8.99 \pm 1.43) \times 10^{-6}$	4
Dexamethasone	$(2.42 \pm 1.03) \times 10^{-5}$	7
Metronidazole	$(1.59 \pm 0.43) \times 10^{-5}$	5

Table 6 Permeability coefficient of agent in rabbit sclera [46]

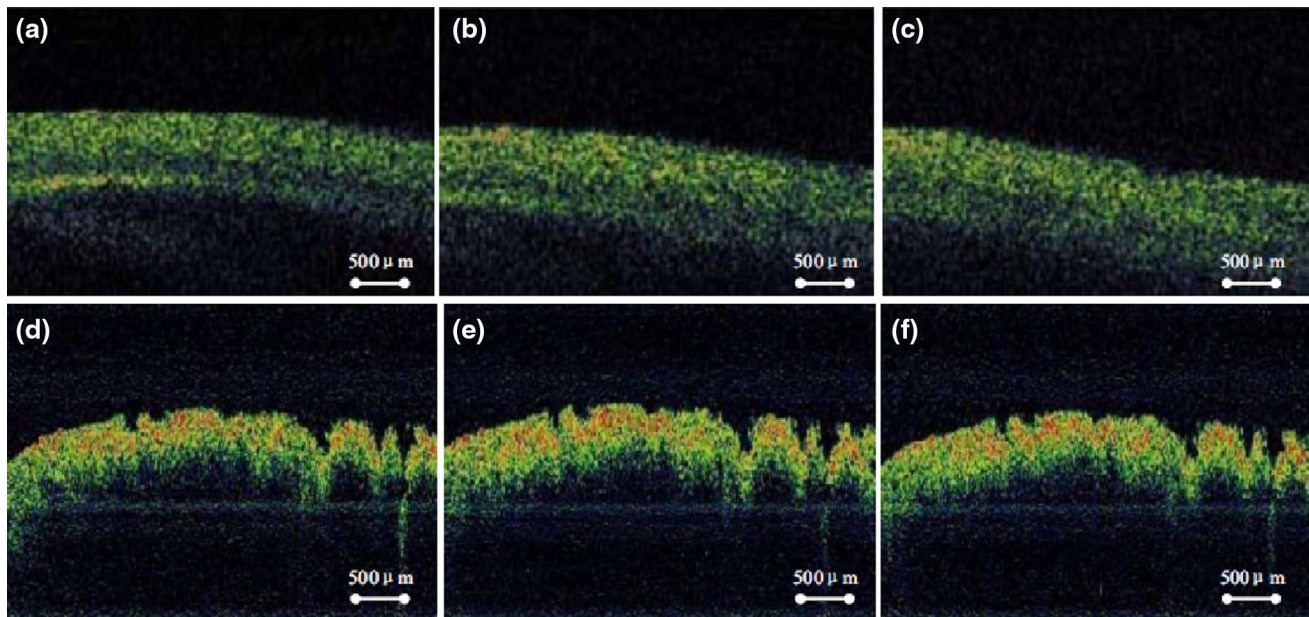| Agent	Permeability coefficient ± SD (cm/s)	No. of independent experiments
Water	$(1.33 \pm 0.28) \times 10^{-5}$	5
Ciprofloxacin	$(1.41 \pm 0.38) \times 10^{-5}$	3
Mannitol	$(6.18 \pm 1.08) \times 10^{-6}$	5
Dexamethasone	$(864 \pm 1.12) \times 10^{-6}$	14
Metronidazole	$(1.31 \pm 0.29) \times 10^{-5}$	4

Fig. 13 Normal stomach OCT images (**a–c**) and tumor-induced OCT images (**d–f**) at 0, 20, and 40 min during the 20 % glucose diffusion experiment (reprinted with permission [50])

glucose in the normal esophagus and esophageal squamous cell carcinoma (ESCC) tissues was calculated by using the OCTSS method. The monitored region of the tissue was about 210 μm in thickness and 290 μm away from the surface. It took 35 min to reach the glucose in the monitored region and 67 min to completely diffuse. This information gives the average permeability coefficient of 40 % glucose solution from different normal esophageal tissues to be $(1.74 \pm 0.04) \times 10^{-5}$ cm/s. In the similar fashion, the permeability coefficient of 40 % glucose in ESCC tissues was found to be $(2.45 \pm 0.06) \times 10^{-5}$ cm/s [49].

Larin et al. [19] used the fiber-optic-based OCT setup for blood glucose monitoring in human skin. This slope analysis provides the best correlation in the range from 200 to 600 μm. In this way, four consecutive OCT signals were averaged, normalized, and plotted as a function of time. The depth investigated in this work was 550–600 μm and 380–500 μm. Seventeen percentage of change in the slope have been observed with the changes in glucose concentration, from 90 to 140 mg/dl, in one volunteer and ~15 % with the changes in glucose concentration, from 100 to 200 mg/dl, in the other volunteer [19].

1.6.2 Hyperosmotic agent in gastric cancer

To observe the dynamic diffusion of the hyperosmotic agent in normal and atherosclerotic aortic tissues, two stages have been observed, i.e., from the top tissue to the intercellular space and into the cell matrix. By introducing the dehydration, the imaging contrast can be improved during the first stage. For this monitoring and quantification by permeability coefficients of hyperosmotic agents, the diffusion of 20 % aqueous solution of glucose in tumor tissues has been used. The OCT system used in this experiment consists of SLD ($\lambda_0 = 830$ nm, $\Delta\lambda = 50$ nm, axial resolution of 10–15 μm, transverse resolution of 20 μm, SNR ~100 dB). The signal is guided through visible light source of 645 nm. Each A-scan consists of 10,000 data points, and the time consumed for lateral scanning is ~1.0 s. The permeability coefficient of glucose in tissues ex vivo is measured with OCTSS method [46]. The OCT images of the normal stomach tissues ex vivo at 0, 20, and 40 min during the 20 % glucose diffusion experiment are shown in Fig. 13a–c, respectively. Here, we can see the submucosal layers of normal stomach tissues with layer structures at 0 and 20 min. The stomach tumor tissues ex vivo are shown in Fig. 13d–f by showing the destruction of layer structures in the gastric cancer tissues. The equilibrium is set up after this 20 min thus giving permeability coefficients of $0.94 \pm 0.04 \times 10^{-5}$ cm/s. With the same procedure, the permeability coefficient is found for defective tissue $5.32 \pm 0.17 \times 10^{-5}$ cm/s. The two types of tissues investigated in this experiment give a decrease in permeability coefficient in tumor [50].

1.6.3 Effect of skin pressure on blood glucose monitoring

The effect of pressure on biological tissues yields the following extractions: (i) Blood and interstitial fluid volume

are reduced [51], (ii) light transmission increases due to thickness reduction [52], and (iii) the vasodilation [53]. The motion artifacts for in vivo experiments can be reduced by placing OCT probe on the skin and applying a slight pressure to the probe. Consequently, a drift in the slope of the OCT signal is observed during blood glucose monitoring due to this pressure [54].

References

1. E.A. Swanson, D. Huang, M.R. Hee, J.G. Fujimoto, C.P. Lin, C.A. Puliafito, Opt. Lett. **17**, 151 (1992)
2. C.A. Puliafito, J.S. Schuman, M.R. Hee, J.G. Fujimoto, *Optical coherence tomography of ocular diseases*. (SLACK Inc., 1996)
3. D. Stifter, Appl. Phys. B **88**, 337–357 (2007)
4. J. Czajkowski, T. Fabritius, J. Ulański, T. Marszałek, M. Gazicki-Lipman, A. Nosal, R. Śliż, E. Alarousu, T. Prykäri, R. Myllylä, G. Jabbour, Appl. Phys. B **105**, 649–657 (2011)
5. S. Yazdanfar, J.A. Izatt, Opt. Lett. **27**, 2085–2087 (2002)
6. H. Ullah, B. Davoudi, A. Mariampillai, G. Hussain, M. Ikram, I. Vitkin, Laser Phys. **22**, 797–804 (2012)
7. H. Ullah, A. Mariampillai, M. Ikram, I. Vitkin, Laser Phys. **21**, 1962–1971 (2011)
8. P. Zakharov, M.S. Talary, I. Kolm, A. Caduff, Physiol. Meas. **31**, 193 (2010)
9. O.S. Khalil, Diabetes Technol. Ther. **6**, 660–697 (2004)
10. E.H. Yoo, S.Y. Lee, Sensors **10**, 4558–4576 (2010)
11. O.K. Cho, Y.O. Kim, H. Mitsumaki, K. Kuwa, Clin. Chem. **50**, 1894–1898 (2004)
12. M.G. Ghosn, V.V. Tuchin, K.V. Larin, Opt. Lett. **31**, 2314–2316 (2006)
13. G.L. Cote, M.D. Fox, R.B. Northrop, IEEE Trans. Biomed. Eng. **39**, 752–756 (1992)
14. Y. Liu, P. Hering, M.O. Scully, Appl. Phys. B **54**, 18–23 (1992)
15. M.R. Prausnitz, J.S. Noonan, J. Pharm. Sci. **87**, 1479–1488 (1998)
16. R.A. Gabbay, S. Sivarajah, Diabetes Technol. Ther. **10**, 188–193 (2008)
17. R. Poddar, J. T. Andrews, P. Shukla, P. Sen, arXiv:0810.5755 1–47 (2008)
18. B. Ramamurthy, P. Höök, A.D. Jones, L. Larsson, FASEB J. **15**, 2415–2422 (2001)
19. K.V. Larin, M.S. Eledrisi, M. Motamedi, R.O. Esenaliev, Diabetes Care **25**, 2263–2267 (2002)
20. R.O. Esenaliev, K.V. Larin, I.V. Larina, M. Motamedi, Opt. Lett. **26**, 992–994 (2001)
21. M.Y. Kirillin, A.V. Priezzhev, M. Kinnunen, E. Alarousu, Z. Zhao, J.T. Hast, R.A. Myllyl, Opt. Diagn. Sens. IV. 164–173 (2004). doi:10.1117/12.535341
22. M. Kinnunen, R. Myllylä, T. Jokela, S. Vainio, Appl. Opt. **45**, 2251–2260 (2006)
23. K.V. Larin, T.V. Ashitkov, I.V. Larina, I.Y. Petrova, M.S. Eledrisi, M. Motamedi, R.O. Esenaliev, Optical coherence tomography and noninvasive blood glucose monitoring: a review. in *Proc. SPIE 5474, Saratov Fall Meeting 2003: Optical Technologies in Biophysics and Medicine V*, vol. 285 (2004). doi:10.1117/12.578965
24. F. Shu, Y. Kehong, Y. Datian. International Conference on Information Technology and Applications in Biomedicine (ITAB) (2008)
25. V.L. Kirill, M. Massoud, V.A. Taras, O.E. Rinat, Phys. Med. Biol. **48**, 1371 (2003)
26. K.V. Larin, M.S. Eledrisi, M. Motamedi, R.O. Esenaliev, Diabetes Care **25**, 2263–2267 (2002)
27. V. Sapozhnikova, R. Kuranov, D. Prough, I. Cicenaite, R. Esenaliev, Opti. Soc. Am. MC3 (2006)
28. H. Ullah, M. Atif, S. Firdous, M.S. Mehmood, M. Ikram, C. Kurachi, C. Grecco, G. Nicolodelli, V.S. Bagnato, Laser Phys. Lett. **7**, 889–898 (2010)
29. K.V. Larin, M.G. Ghosn, S.N. Ivers, A. Tellez, J.F. Granada, Laser Phys. Lett. **4**, 312–317 (2007)
30. H. Ullah, G. Gilanie, M. Attique, M. Hamza, M. Ikram, Laser Phys. **22**, 1002–1010 (2012)
31. B.J. Berne, R. Pecora, *Dynamic Light Scattering: With Applications to Chemistry, Biology, and Physics*, (Dover Publications 2013)
32. A. Mariampillai, M.K.K. Leung, M. Jarvi, B.A. Standish, K. Lee, B.C. Wilson, A. Vitkin, V.X.D. Yang, Opt. Lett. **35**, 1257–1259 (2010)
33. H. Ullah, *Imaging of Biological Tissues using Diffuse Reflectance and Optical Coherence Tomography*, in *Department of Physics*, Pakistan Institute of Engineering and Applied Sciences: Islamabad. (2012) p. 152
34. K.K. Bizheva, A.M. Siegel, D.A. Boas, Phys. Rev. E **58**, 7664 (1998)
35. M.E. Brezinski, *Optical Coherence Tomography: Principles and Applications,* (Elsevier Science 2006)
36. N. Dobrovol'skii, Y. Lopukhin, A. Parfenov, A. Peshkov, Biomed. Eng. **31**, 140–143 (1997)
37. http://www.epakmachinery.com/products/viscosity-chart. cited 28 Jan 2011
38. M. Ninck, M. Untenberger, T. Gisler, Biomed. Opt. Express **1**, 1502–1513 (2010)
39. Z. Li, H. Li, J. Li, X. Lin, Laser Phys. **21**, 1995–1998 (2011)
40. H. Ullah, E. Ahmed, M. Ikram, JETP Lett. **97**, 690–696 (2013)
41. H. Ullah, M. Ikram, *Optical Coherence Tomography for Glucose Monitoring in Blood*. (LAP Lambert, Academic Publishing, 2012)
42. N. Sudheendran, S.H. Syed, M.E. Dickinson, I.V. Larina, K.V. Larin, Laser Phys. Lett. **8**, 247–252 (2011)
43. R. Ballerstadt, A. Kholodnykh, C. Evans, A. Boretsky, M. Motamedi, A. Gowda, R. McNichols, Anal. Chem. **79**, 6965–6974 (2007)
44. K.V. Larin, V.V. Tuchin, Quantum Electron. **38**, 551 (2008)
45. M.G. Ghosn, N. Sudheendran, M. Wendt, A. Glasser, V.V. Tuchin, K.V. Larin, J. Biophotonics **3**, 25–33 (2010)
46. M.G. Ghosn, V.V. Tuchin, K.V. Larin, Invest. Ophthalmol. Vis. Sci. **48**, 2726–2733 (2007)
47. K.V. Larin, M.G. Ghosn, S.N. Ivers, A. Tellez, J.F. Granada, Laser Phys. Lett. **4**, 312 (2007)
48. M.G. Ghosn, S.H. Syed, N.A. Befrui, M. Leba, A. Vijayananda, N. Sudheendran, K.V. Larin, Laser Phys. **19**, 1272–1275 (2009)
49. Q.L. Zhao, J.L. Si, Z.Y. Guo, H.J. Wei, H.Q. Yang, G.Y. Wu, S.S. Xie, X.Y. Li, X. Guo, H.Q. Zhong, L.Q. Li, Laser Phys. Lett. **8**, 71–77 (2011)
50. H. Xiong, Z. Guo, C. Zeng, L. Wang, Y. He, S. Liu, J. Biomed. Optics **14**, 024029–024029 (2009)
51. V.T. Valery, J. Phys. D Appl. Phys. **38**, 2497 (2005)
52. A. Vogel, C. Dlugos, R. Nuffer, R. Birngruber, Lasers Surg. Med. **11**, 331–340 (1991)
53. V.V. Sapozhnikova, R.V. Kuranov, I. Cicenaite, R.O. Esenaliev, D.S. Prough, J. Biomed. Optics **13**, 021112–021112 (2008)
54. V.K. Roman, V.S. Veronika, S.P. Donald, C. Inga, O.E. Rinat, Phys. Med. Biol. **51**, 3885 (2006)